

PushAround: Collaborative Path Clearing via Physics-Informed Hybrid Search

Abstract—The passage of large vehicles in cluttered environments is often blocked by movable obstacles, motivating the use of mobile robot teams to proactively clear traversable corridors. Existing approaches to Navigation Among Movable Obstacles (NAMO) mainly plan abstract sequences of obstacle displacements but neglect physical feasibility, overlooking robot dimensions, obstacle mass, contact geometry, and required forces, which often leads to strategies that fail in execution. This work introduces PushAround, a physics-informed framework that guarantees feasible path clearing by coupling geometric reasoning with dynamic validation. The core novelty is a hybrid search that jointly determines which obstacles to displace and how to push them, including contact points, directions, and forces. The framework builds a W-Clearance Connectivity Graph (WCCG) to test vehicle passage, ranks frontier gaps to prioritize obstacle-clearing actions, and incrementally expands feasible plans by validating pushing modes. This integration ensures that solutions are both geometrically valid and physically executable. Efficiency is achieved by combining compact geometric reasoning with prioritized evaluation, avoiding exhaustive simulation and improving scalability beyond prior NAMO methods. Extensive simulations and hardware experiments demonstrate robust success, physical validity, and superior efficiency compared to state-of-the-art approaches.

I. INTRODUCTION

In many real-world settings, the passage of large vehicles or transport units is obstructed by movable obstacles such as pallets, boxes, or equipment, motivating the deployment of mobile robot teams to actively clear traversable corridors and enable safe passage. This capability is particularly critical in cluttered and unstructured environments—warehouses, disaster sites, and dense urban spaces—where conventional path planning methods assume static obstacles and thus fail once direct routes are blocked [1]. Navigation Among Movable Obstacles (NAMO) has been studied as a means of creating new routes by pushing, pulling, or rotating obstacles [2], yet most existing methods abstract away physical feasibility. Factors such as robot dimensions, obstacle size and mass, contact geometry, applied forces, and the coupled dynamics of pushing are typically ignored, producing plans that are geometrically valid but physically unrealizable. The difficulty is amplified by the fact that a single large robot is often unable to clear a corridor unaided, smaller robots are limited by their reach and access to obstacle boundaries, and cooperative pushing introduces strong physical coupling where one action can trigger chained motions of multiple obstacles, making prediction and planning substantially more complex.

A. Related Work

Navigation Among Movable Obstacles (NAMO) has been studied as an extension of motion planning in cluttered



Fig. 1. Snapshots of collaborative path clearing system in both simulation and hardware. A team of robots actively reconfigures movable obstacles to create a W -clear path for a large vehicle to traverse from start to goal.

environments. Classical methods planned explicit sequences of obstacle displacements through pushing, pulling, or rotating [2], [3], while later work introduced heuristic search for scalability [3] and graph- and sampling-based formulations for larger workspaces [4]. Recent efforts extend NAMO to multi-agent settings where teams of robots clear passages collaboratively [5], [6]. However, most NAMO approaches still idealize robots as point agents with unlimited actuation and neglect robot size, obstacle mass, and realistic dynamics, which leads to plans that are geometrically valid but physically unrealizable.

Collaborative pushing has also been widely investigated in multi-robot manipulation. Foundational studies examined the mechanics of pushing and the limit surface model [7], [8], while more recent work addressed force synchronization [9], contact stability and slip margins [10], [11], and cooperative transport of large payloads in structured environments [12], [13]. Learning-based approaches have further explored emergent coordination in cluttered settings [14]. These studies demonstrate effective multi-robot cooperation but are generally limited to single-object tasks and assume strict collision avoidance with surrounding obstacles. As a result, inter-object interactions and the coupled dynamics of multiple movable obstacles remain largely unaddressed.

Physics-informed planning has emerged to integrate realistic dynamics into motion generation. Several methods use physics engines to validate candidate manipulations [15] or embed contact simulation directly in the planning loop [16]. Other approaches incorporate dynamic models into planning for non-prehensile manipulation [?], [17] or apply learning

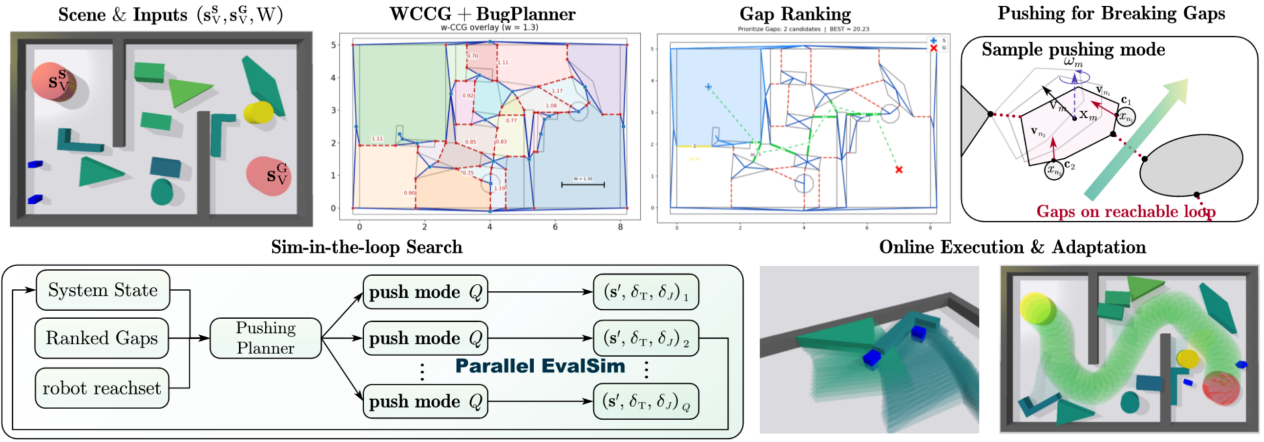


Fig. 2. Illustration of the W-Clearance Connectivity Graph (WCCG). **Left:** Cluttered PyBullet scenario with the immovable walls and movable objects; **Middle:** WCCG overlay with the centroid nodes (blue squares), bridge nodes (red circles), centroid–bridge edges (blue), and bridge–bridge edges (red dashed) annotated by the gap widths; **Right:** Induced faces of the WCCG, where the colors indicate distinct connected regions.

with physics priors and differentiable physics for contact-rich tasks [18], [?], [9], [10]. While these approaches highlight the benefits of embedding physical reasoning, they often decouple high-level planning from low-level feasibility checks or remain confined to single-object manipulation. Consequently, they do not scale to collaborative path clearing in cluttered environments with many movable obstacles.

B. Our Method

This work introduces *PushAround*, a physics-informed framework for collaborative multi-robot pushing that actively constructs traversable corridors for large vehicles in cluttered environments. The central novelty is a hybrid search that jointly determines which obstacles to displace and how to push them, coupling the high-level sequence of obstacle-clearing actions with low-level pushing modes that specify contact points, directions, and forces. The framework integrates three components: a W-Clearance Connectivity Graph (WCCG) that certifies vehicle passage under width constraints, a gap-ranking strategy that prioritizes frontier gaps by estimated effort, and a search procedure that incrementally expands candidate plans while validating their physical realizability. This integration guarantees that the resulting plans are not only geometrically valid but also feasible under robot dimensions, object mass, contact geometry, and coupled pushing dynamics. Efficiency is achieved by combining compact geometric reasoning with prioritized evaluation, focusing computation on the most promising actions and avoiding the scalability issues of simulation-heavy NAMO approaches.

The contributions of this work are twofold: (I) it introduces the first unified framework that couples multi-robot collaborative pushing with physics-informed feasibility guarantees, producing executable plans for path clearing in dense cluttered environments; and (II) it demonstrates significant improvements in feasibility, efficiency, and scalability over existing NAMO and collaborative pushing methods, through extensive simulation and hardware validation.

II. PROBLEM DESCRIPTION

A. Workspace and Robots

The workspace is a bounded planar region $\mathcal{W} \subset \mathbb{R}^2$ that contains two types of obstacles. A set \mathcal{O} represents immovable structures, while a set of M movable rigid polygons is defined as $\Omega \triangleq \{\Omega_1, \dots, \Omega_M\} \subset \mathcal{W}$. Each movable obstacle Ω_m is characterized by its mass M_m , inertia I_m , frictional parameters (either identified or estimated), and state $s_m(t) \triangleq (\mathbf{x}_m(t), \psi_m(t))$, where $\mathbf{x}_m(t) \in \mathbb{R}^2$ is the planar position of its centroid and $\psi_m(t) \in \mathbb{R}$ its orientation angle. The region occupied by Ω_m at time t is denoted $\Omega_m(t)$. Moreover, a small team of N robots, indexed as $\mathcal{R} \triangleq \{R_1, \dots, R_N\}$, operates as a cooperative unit. Each robot R_i is modeled as a rigid body with state $s_{R_i}(t) \triangleq (\mathbf{x}_{R_i}(t), \psi_{R_i}(t))$, where $\mathbf{x}_{R_i}(t) \in \mathbb{R}^2$ is its position and $\psi_{R_i}(t) \in \mathbb{R}$ its orientation. The footprint of R_i is denoted $R_i(t)$. The instantaneous free space is given by:

$$\widehat{\mathcal{W}}(t) \triangleq \mathcal{W} \setminus \left(\mathcal{O} \cup \{\Omega_m(t)\}_{m=1}^M \cup \{R_i(t)\}_{i=1}^N \right), \quad (1)$$

where $\widehat{\mathcal{W}}(t)$ excludes regions occupied by immovable obstacles, movable obstacles, and robots.

B. External Vehicle and Clearance Goal

An external vehicle V of radius $W/2 > 0$ must navigate within the workspace from a start configuration s_V^S to a goal configuration s_V^G . Since movable obstacles may obstruct the way, a direct passage is not always feasible. Feasibility at time t is captured by the W -clearance condition

$$\exists \mathcal{P}_V^W \subset \widehat{\mathcal{W}}(t) : s_V^S \leadsto s_V^G, \text{clr}(\mathcal{P}_V^W) \geq W, \quad (2)$$

where \mathcal{P}_V^W is a continuous curve connecting start and goal inside the free space, and $\text{clr}(\mathcal{P}_V^W)$ denotes its minimum clearance to surrounding obstacles.

C. Collaborative Pushing Modes

Thus, the robots may actively reconfigure Ω by pushing obstacles. The interaction with obstacle Ω_m is described by a pushing mode $\xi_m \triangleq (\mathcal{C}_m, \mathbf{u}_m)$, where $\mathcal{C}_m \in (\partial\Omega_m)^N$ is the set of contact points established by the robots, and $\mathbf{u}_m \in \mathbb{R}^{2N}$

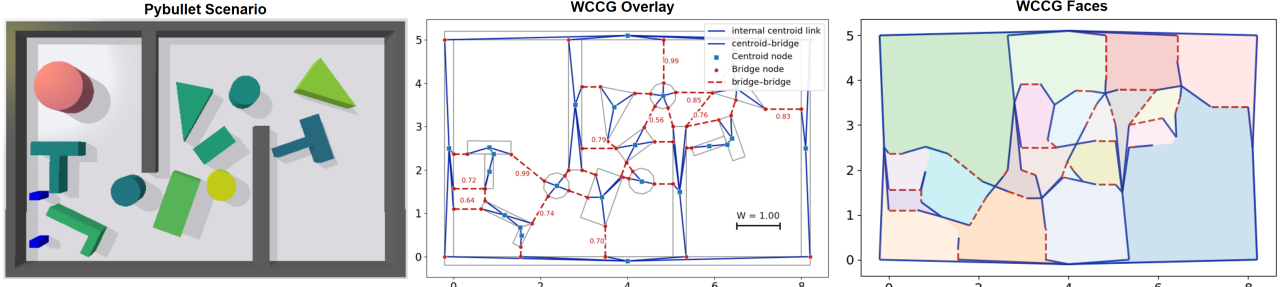


Fig. 3. Illustration of the W-Clearance Connectivity Graph (WCCG). **Left:** Cluttered PyBullet scenario with the immovable walls and movable objects; **Middle:** WCCG overlay with the centroid nodes (blue squares), bridge nodes (red circles), centroid-bridge edges (blue), and bridge-bridge edges (red dashed) annotated by the gap widths; **Right:** Induced faces of the WCCG, where the colors indicate distinct connected regions.

encodes the body-frame forces or an equivalent wrench profile. The admissible set of modes is Ξ_m , determined by contact geometry and frictional limits. Furthermore, the system evolution under a pushing mode is captured by the transition operator below:

$$\mathbf{S}(t^+) \triangleq \Phi(\mathbf{S}(t), m, \xi_m), \quad (3)$$

where $\mathbf{S}(t)$ stacks all robot and obstacle states. The operator Φ models the joint dynamics of robots and obstacles under contact. In general, Φ is not available in closed form and is instead evaluated through physics simulation.

D. Problem Statement

The goal is to compute a hybrid schedule for the robots that reconfigures the movable obstacles so that the vehicle admits a W -feasible path from start to goal. The overall schedule for the robotic fleet is defined as:

$$\pi \triangleq \{(m_k, \xi_k, \Delta t_k)\}_{k=1}^K, \quad (4)$$

where $\Omega_{m_k} \in \Omega$ specifies the movable obstacle to manipulate, $\xi_k \in \Xi_{m_k}$ is the pushing mode, and $\Delta t_k > 0$ the duration of execution. Thus, the optimization problem balances the execution time and the physical effort of the clearance process, subject to various constraints, i.e.,

$$\min_{\pi} \left\{ T + \alpha \sum_{k=1}^K J(m_k, \xi_k, \mathbf{S}(\tau_k)) \right\}, \quad (5)$$

where $T \triangleq \sum_{k=1}^K \Delta t_k$ is the total task duration, $\alpha > 0$ is a trade-off parameter, and $J(\cdot)$ is a simulation-based control effort or feasibility cost evaluated at state $\mathbf{S}(\tau_k)$. Note that the above optimization problem is constrained by (1), (2), and (3), which jointly ensure collision-free evolution within the workspace, valid dynamic transitions under pushing, and a terminal W -clearance path for the vehicle.

Remark 1. Problem (5) above uniquely couples obstacle selection, pushing modes, and timing into a single hybrid optimization. This yields a combinatorial search space far more complex than classical NAMO, where prior work often assumes simple object shapes or hand-crafted contact modes [13], [7], [11], [19]. ■

III. PROPOSED SOLUTION

The unified framework called PushAround is developed to enable collaborative multi-robot pushing with physical feasibility, as described in this section. The framework begins by constructing a W-Clearance Connectivity Graph, introduced in Sec. III-A, which captures the connectivity of the workspace under the clearance requirement and identifies frontier gaps that block passage. Building on this representation, Sec. III-B presents a gap-ranking strategy that assigns costs to candidate gaps and determines which obstacle-clearing actions are most promising. These ranked actions are then evaluated within a simulation-in-the-loop search, described in Sec. III-C, where a configuration-space tree is expanded and candidate pushes are validated by parallel physical simulation. The complete execution flow together with generalization aspects is summarized in Sec. III-D.

A. W-Clearance Connectivity Graph

The feasibility of routing the vehicle depends on whether a corridor of width W exists between the start configuration s_v^S and the goal configuration s_v^G . To address this question, a *W-Clearance Connectivity Graph* (WCCG) is introduced. The WCCG encodes adjacency relations between obstacles under the clearance threshold W and supports efficient connectivity queries. Unlike grid maps or sampled roadmaps, it is constructed directly from obstacle geometry, avoiding discretization errors and ensuring consistent results. This is particularly important since clearance queries must be invoked repeatedly during planning.

1) *Graph Construction:* The WCCG is built by decomposing each movable obstacle $\Omega_m \in \Omega$ into convex components. From each component C , a centroid node v_c is created. When two components C_u and C_v have closest points $p_u \in C_u$ and $p_v \in C_v$ with distance smaller than W , bridge nodes are added at p_u and p_v . These bridge nodes are connected by a bridge-bridge edge, annotated with the corresponding gap width $w_{uv} \triangleq \|p_u - p_v\|$, and further linked back to their centroids with centroid-bridge edges. Narrow passages with $w_{uv} < W$ are explicitly marked as potential bottlenecks. The resulting graph is defined below:

$$\mathcal{G}_W \triangleq (\mathcal{V}, \mathcal{E}_c \cup \mathcal{E}_b), \quad (6)$$

where \mathcal{V} contains all centroid and bridge nodes; \mathcal{E}_c is the set of centroid-bridge edges; and \mathcal{E}_b the set of bridge-bridge edges annotated by widths w_{uv} .

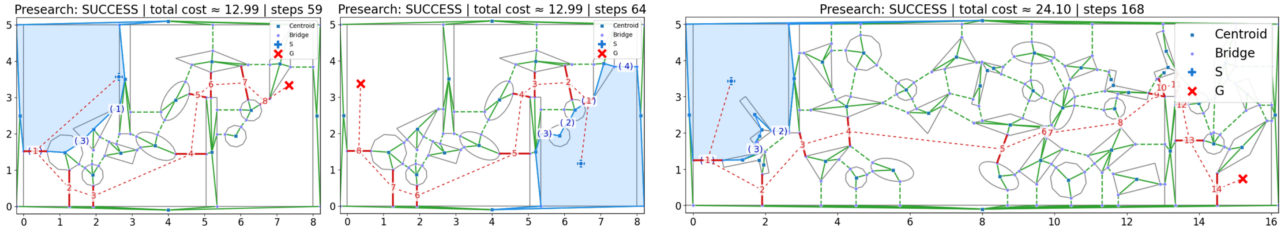


Fig. 4. Illustration for the ranking of potential gaps. Each panel shows the WCCG with the current face (light blue). The algorithm (i) extracts the frontier loop from BugPlanner, (ii) enumerates candidate bridge–bridge gaps on the loop, (iii) assigns local first-hop ranks (blue numbers), and (iv) simulates a short presearch to predict the full gap-crossing sequence (red numbers). **Top:** start/goal swapped in the same map \Rightarrow symmetric sequences, predicted cost 12.99. **Bottom:** larger map (~ 30 obstacles) with a 14-gap sequence, predicted cost 24.10.

2) *Connectivity Criterion*: Once \mathcal{G}_W has been constructed, connectivity queries can be performed without explicitly computing a geometric path. A frontier-tracing procedure, similar to the BugPlanner [20], starts from the vehicle start s_v^S , casts a ray toward the goal s_v^G , and explores the encountered loop of frontier edges. If a valid exit is discovered, the process continues until the goal is reached; otherwise a blocking cycle is returned. Successful execution produces a skeleton Σ , which is an ordered sequence of centroid and bridge nodes that certifies s_v^S and s_v^G lie in the same connected face. Let the W -clear free space be $\mathcal{F}_W \triangleq \mathbb{R}^2 \setminus (\mathcal{O} \oplus \mathbb{B}_{W/2})$, where \oplus denotes Minkowski addition and $\mathbb{B}_{W/2}$ is a closed disk of radius $W/2$. A complete criterion for existence of a W -clear path \mathcal{P}_v^W is defined as:

$$\exists \mathcal{P}_v^W \subset \mathcal{F}_W : s_v^S \rightsquigarrow s_v^G \iff \left\{ \begin{array}{l} s_v^S, s_v^G \text{ belong to the} \\ \text{same face of } \mathcal{G}_W; \mathbb{B}_{W/2}(s_v^S), \mathbb{B}_{W/2}(s_v^G) \subset \mathcal{F}_W \end{array} \right\}, \quad (7)$$

where $\mathbb{B}_{W/2}(\cdot)$ denotes a disk of radius $W/2$ centered at the argument. They align with (2) for the external vehicle.

3) *Skeleton to Path*: The skeleton Σ as an output of the previous step, is an ordered sequence of centroid and bridge nodes connected by frontier edges in \mathcal{G}_W . This skeleton serves as a compact certificate that s_v^S and s_v^G lie in the same connected face. Given as input the skeleton Σ , together with \mathcal{G}_W , the clearance W , and the endpoint disks $\mathbb{B}_{W/2}(s_v^S)$ and $\mathbb{B}_{W/2}(s_v^G)$, the output is an explicit W -clear path \mathcal{P}_v^W . This path is constructed by sliding each skeleton segment along the boundary of the inflated obstacles, offsetting slightly inward into \mathcal{F}_W , and attaching short connectors inside the endpoint disks. The resulting \mathcal{P}_v^W remains in \mathcal{F}_W , preserves the homotopy of Σ , and guarantees clearance of at least W .

Remark 2. The proposed WCCG differs from sampling- and grid-based planners in two key aspects: (I) It avoids discretization of \mathcal{W} and is therefore free from resolution-induced errors; (II) It relies purely on geometry, which makes queries highly efficient. These two features are crucial, since connectivity checks and clearance tests are invoked many times within the hybrid planner described in the sequel. ■

B. Ranking of Potential Blocking Gaps

When the condition in (7) fails, the vehicle cannot reach s_v^G from s_v^S through a W -clear path \mathcal{P}_v^W . In this case, the planner must prioritize *blocking gaps* on the reachable frontier of \mathcal{G}_W . The goal of this module is to provide an ordered list of

such gaps, ranked by their predicted cost to eventually yield a feasible path, which serves as a critical guidance for the hybrid search in the sequel.

1) *Frontier Extraction and Candidate Gaps*: A BugPlanner query on \mathcal{G}_W , given (s_v^S, s_v^G, W) , either confirms connectivity or returns a counter-clockwise frontier loop \mathcal{L} that separates the two endpoints. The bridge–bridge edges visible on \mathcal{L} form the first-hop candidate set $\Gamma_{\mathcal{L}} \triangleq \{g_1, \dots, g_K\}$, where each g_k is a reachable candidate gap. These candidates are the inputs to the ranking module, while the output will be an ordered list of the same set sorted by predicted cost.

2) *Evaluation for Immediate Cost*: Each candidate $g \in \Gamma_{\mathcal{L}}$ is evaluated by combining the cost for the robots to reach the gap and the effort required to widen it. Let $\mathbf{s}_{\mathcal{R}}$ be the current robot positions, and \mathbf{o}_g as the outside insertion point of gap g . The resulting one-hop cost is given by:

$$C(g | \mathcal{L}, \mathbf{s}_{\mathcal{R}}) = \lambda_t C_t(\mathbf{s}_{\mathcal{R}}, \mathbf{o}_g) + \lambda_p C_p(g), \quad (8)$$

where $\lambda_t, \lambda_p > 0$ are weighting factors for the transition and pushing costs, respectively; function $C_t(\cdot)$ denotes the collision-free distance between two points; and the function $C_p(\cdot)$ measures the widening effort, which increases when the gap is narrower than W , or when the adjacent obstacles are heavier as scaled by the mass of adjacent movable obstacles.

3) *Long-term Cost w.r.t. Goal*: Furthermore, to prioritize gaps closer to the goal, a heuristic is added to the evaluation, i.e., $h(g) = \eta \|\mathbf{o}(g) - s_v^G\|$, where $\eta > 0$ is a scaling constant. Lastly, a short A*-style presearch virtually crosses each candidate gap, recomputes the next frontier, and continues for a limited beam width and depth. The predicted cost-to-connect is given by:

$$\widehat{Cost}(g) \triangleq C(g | \mathcal{L}, \mathbf{s}_{\mathcal{R}}) + \sum_{g' \in \Pi^*(g)} \{C(g' | \cdot) + h(g')\}, \quad (9)$$

where $\Pi^*(g)$ is the sequence of subsequent gaps discovered after virtually crossing g ; the dots indicate updated inputs along that rollout; and the scalar score $\widehat{Cost}(g) > 0$ for each candidate gap. Consequently, the final output of this module is the ranked list of candidate gaps, i.e., $\text{Rank}(\Gamma_{\mathcal{L}}) \triangleq \text{argsort}_{g \in \Gamma_{\mathcal{L}}} \widehat{Cost}(g)$, which sorts $\Gamma_{\mathcal{L}}$ in ascending predicted cost. This ordered set is passed to the hybrid search module, such that only the promising gaps are expanded first.

Remark 3 (Practical Improvement). Efficiency of the above ranking procedure can be improved by caching frontier loops,

Algorithm 1: Physics-Informed Hybrid Search

Input: $s_0, \alpha, \text{EvalSim}(\cdot), W$ -criterion by (7)

Output: π^*

```

/* Initialization */ ν₀ ← (s₀, ∅), χ(ν₀) = 0;
1 Init Q by (10);
2 while not terminated do
    /* Selection */ ν ← Q.pop_min() by (10);
    /* Parallel Expansion */ foreach g ∈ Rank(ν) do
        foreach (v, ξ) ∈ E_g do
            τ = (g, v, ξ);
            (s', δₜ, δⱼ) ← EvalSim(ν, τ) by (11);
            if success then
                ν' ← (s', π ∪ {τ});
                χ(ν') ← χ(ν) + δₜ + α δⱼ;
                Q.push(ν');
            /* Termination Check */ if s' admits P_v^W by (7) then
                π* ← π', break;
15 return π*;
```

storing the transitions $(\mathcal{L}, g) \mapsto \mathcal{L}'$, and accelerating the edge queries with axis-aligned bounding-box culling. With a small beam width and depth (typically around 8), the runtime of ranking remains negligible compared to the cost of simulation-based validation. ■

C. Physics-Informed Hybrid Search

The hybrid search couples high-level decisions about blocking gaps with low-level feasibility of multi-robot pushing. Unlike purely geometric planners, this procedure simultaneously determines a sequence of gaps to clear and physically feasible pushing actions, including directions, contact modes, and forces. Parallel physics simulation is embedded so that many candidate push strategies can be evaluated simultaneously at each expansion, and the resulting successor states are returned to the search. This tight coupling of discrete graph reasoning with continuous pushing dynamics is unique for the considered problem.

1) *Tree and Initialization:* The search tree \mathcal{T} is composed of nodes $\nu \triangleq (s, \pi)$, where s is the current system state including the positions and orientations of all robots and movable obstacles as in (3), and π is the partial pushing strategy realized so far as in (4). Two global functions are maintained: $\text{Rank}(\nu)$ stores a ranked list of candidate gaps at this node together with their exploration status, derived from (9); and $\chi(\nu)$ returns the cumulative execution cost from the root to ν . The root is initialized as $\nu_0 \triangleq (s_0, \emptyset)$, where S^S corresponds to the initial system state s_0 . At initialization, $\chi(\nu_0) = 0$, and $\text{Rank}(\nu_0)$ is constructed by first computing the frontier loop \mathcal{L}_ν associated with s_0 , then extracting the visible gaps $\Gamma_{\mathcal{L}_\nu}$, and finally ranking them by their predicted cost-to-connect.

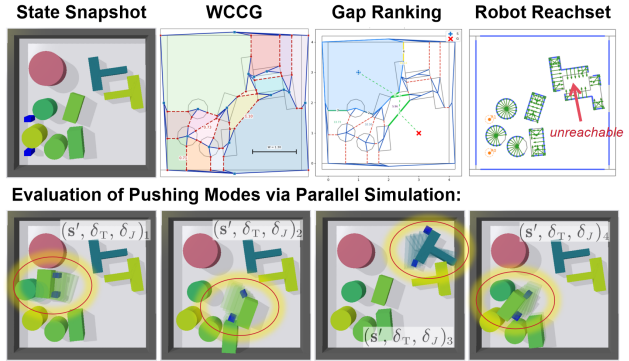


Fig. 5. Overview of PIHS (physics-informed hybrid search). **Top row (four panels):** (1) current simulation snapshot rendered in PyBullet; (2) the corresponding W -clearance connectivity graph (WCCG); (3) presearch on the WCCG with ranked candidate gaps (numbers indicate local/global ranks). **Bottom row:** given the current snapshot, the reachable contacts, and the ranked gaps, PIHS samples push tasks and modes (e.g., face/edge, normal/tangential), executes short-horizon physics rollouts, and visualizes the predicted outcomes: ghosted trails show slider/object trajectories, and the final panel depicts the updated state used for the next search expansion.

2) *Node Selection:* At each iteration, the node with minimum best-first priority is selected from the queue. The priority function balances the realized execution cost and the estimated effort of remaining gaps:

$$f(\nu) \triangleq \chi(\nu) + \min_{g \in \text{Rank}(\nu)} \widehat{\text{Cost}}(g), \quad (10)$$

where $\chi(\nu)$ is the cumulative execution cost so far, and the second term is the minimum predicted remaining cost among the unexplored gaps of ν . This scoring ensures that nodes are expanded in an order that jointly accounts for physical effort already incurred and the most promising future actions.

3) *Node Expansion with Parallel Simulation:* When a node ν is selected for expansion, a batch of *pushing strategies* from $\text{Rank}(\nu)$ is evaluated in parallel by simulation. Each pushing strategy is defined as $\tau \triangleq (g, v, \xi)$, where $g \in \Omega$ is the chosen gap; $v \triangleq (v_x, v_y, \omega) \in \mathbb{R}^3$ is a short-horizon body velocity for the manipulated obstacle; and $\xi \triangleq (\mathcal{C}_m, \mathbf{u}_m) \in (\partial\Omega_m)^N \times \mathbb{R}^{2N}$ is a contact mode specifying robot contact points and pushing forces as in (3). Moreover, each candidate τ is first checked by a geometric quick-pass. If it passes, it is evaluated by the simulator with the current state and pushing strategy:

$$(s', \delta_T, \delta_J) \triangleq \text{EvalSim}(\nu, (g, v, \xi)), \quad (11)$$

where s' is the successor state; $\delta_T > 0$ is the time cost; and δ_J is the control effort as in (5). Thus, a successful evaluation produces a child $\nu' \triangleq (s', \pi')$, where π' is obtained by appending π with τ . The incremental realized cost of τ is $\mathcal{C}(\nu, \tau) \triangleq \delta_T + \alpha \delta_J$, with $\alpha > 0$ the same trade-off parameter as in (5). The cumulative cost is then updated by $\chi(\nu') \triangleq \chi(\nu) + \widehat{\mathcal{C}}(\nu, \tau)$. Since many pushing strategies are simulated concurrently, numerous successors can be expanded in parallel at each iteration.

4) *Termination:* Termination occurs when a node ν reaches a state s for which a W -clear path P_v^W exists from s_V^S to s_V^G , as certified by (7). In this case, the schedule π stored in ν constitutes a complete solution to (5), encoding

both the sequence of gaps to clear and the physically feasible pushing actions that realize them.

Remark 4 (Parallel Expansion and Mode Reuse). Efficiency of the hybrid search stems primarily from parallel evaluation of pushing strategies, which allows many candidate futures to be simulated at once for each expansion. Deferred expansion ensures that nodes with long candidate lists remain in the priority queue until all tasks are attempted. Moreover, validated (\mathbf{v}, ξ) pairs are cached locally within a subtree and stored in a persistent *ModeTable* for reuse across similar obstacles, significantly reducing repeated physics calls. These mechanisms yield orders-of-magnitude speedup relative to naive simulation-based search. ■

D. Overall Analyses

1) *Execution and Online Adaptation*: The output of the hybrid search is a pushing schedule $\pi = \{\tau_1, \dots, \tau_K\}$, where each τ_k specifies a target gap, a short-horizon velocity $\mathbf{v}_k \triangleq (v_x, v_y, \omega)$, and a contact mode ξ_k . Execution proceeds sequentially under a hybrid controller that alternates between transition and pushing phases.

During transition, robots plan collision-free paths in the instantaneous freespace $\widehat{\mathcal{W}}(t)$ to reach their designated contact points. If two paths are imminently head-on, the associated contacts are swapped to avoid deadlock. During pushing, the commanded velocity \mathbf{v}_k is integrated to form a short reference trajectory for the manipulated obstacle. This trajectory is mapped to per-robot contact states using ξ_k , and each robot R_n executes proportional velocity control:

$$\mathbf{v}_n = K_p(\hat{\mathbf{p}}_n^c - \mathbf{p}_n^c), \quad \omega_n = K_r(\hat{\psi}_n^c - \psi_n^c),$$

where $(\hat{\mathbf{p}}_n^c, \hat{\psi}_n^c)$ are the reference contact states, $(\mathbf{p}_n^c, \psi_n^c)$ are the measured states, and $K_p, K_r > 0$ are control gains. Small offsets are adapted online to compensate for yaw drift and maintain stable contact.

Execution is monitored continuously. Transition feasibility is checked by timeouts, while pushing is monitored by early-stop tests. If the commanded widening succeeds, execution advances to τ_{k+1} ; otherwise, the executor returns control to the planner with the current state. At a lower rate, the WCCG is rebuilt and the execution terminates immediately once a W -clear path \mathcal{P}_V^W exists between \mathbf{s}_V^S and \mathbf{s}_V^G .

Remark 5 (Endpoint Booster). The W -CCG criterion of (7) may be conservative near the endpoints. If connectivity holds but the disks $\mathbb{B}_{W/2}(\mathbf{s}_V^S)$ or $\mathbb{B}_{W/2}(\mathbf{s}_V^G)$ intersect obstacles, the planner generates a small set of auxiliary pushes directed away from the endpoints. These pushes clear the disks and allow execution to proceed. ■

2) *Computational Complexity*: The cost of each node expansion is dominated by simulation of pushing strategies. Construction of the W -clearance graph \mathcal{G}_W and the associated connectivity tests scale nearly linearly in the number of movable obstacles $|\Omega|$, while gap ranking by presearch (Sec. III-B) is lightweight because it is limited to a small subset of frontier gaps. At expansion, only a fraction

TABLE I
PERFORMANCE ON THE NOMINAL SCENARIO WITH
PUSH-COUNT (MEAN \pm STD).

Method	Succ. (%)	#PT (s)	#ET (s)	#Sims	#Pushes
DFS-WCCG	25.0	41.8	N/A	—	—
SL-Push (off-line)	62.5	0.03	145.1	0.0	7.0
SL-Push (sim)	75.0	25.1	246.8	16.0	8.0
Rec-NAMO	37.5	10.5	179.3	0.0	7.0
PIHS (ours)	92.5	10.3	28.6	121.5	6.0

Metrics. Succ. = success rate; #PT = planning time; #ET = execution time; #Sims = simulations invoked; #Pushes = length of executed push sequence.

TABLE II
ABLATIONS ON THE NOMINAL SCENARIO (40 TRIALS).

Variant	Succ. (%)	Time (s)	#Sims	#PT / #Sims / Succ.
SiLS (full)	92.5	28.6	122	baseline
w/o presearch	85.0	35.2	178	+6.6 / +56 / -7.5%
w/o ModeTable	80.0	33.4	164	+4.8 / +42 / -12.5%
w/o quick-pass	90.0	41.9	208	+13.3 / +86 / -2.5%
w/o reinsertion	82.5	31.1	151	+2.5 / +29 / -10.0%

of the strategies in $\text{Rank}(\nu)$ survive the geometric quick-pass and early-stop checks, which shortens the horizon of the simulator calls defined by EvalSim. Parallel execution of these simulations across multiple workers reduces the effective cost nearly linearly until communication overhead is reached. Deferred expansion further improves efficiency by distributing the evaluation of $\text{Rank}(\nu)$ across iterations, avoiding redundant restarts and keeping the priority queue focused on promising frontiers.

3) *Generalization*: The framework admits several natural extensions: (I) *Heterogeneous teams*. The controller structure admits per-robot gain tuning, and mode priors can be augmented with robot-specific constraints. This enables heterogeneous robots to cooperate within the same framework; (II) *Concurrent pushing*. While the executor applies one push task at a time, the framework can be extended to allow concurrent pushing of multiple obstacles. Such an extension requires multi-object mode generation and transition planning to account for inter-robot conflicts; (III) *Dynamic environments*. Periodic W -connectivity checks and on-demand re-planning enable adaptation to moderate disturbances such as object drift or unmodeled contacts. The framework can therefore generalize to settings where the environment changes gradually during execution.

IV. NUMERICAL EXPERIMENTS

We evaluate the proposed physics-informed hybrid search(PIHS) in cluttered environments containing both movable and immovable obstacles. All components— W -CCG presearch, frontier extraction, and the *ModeTable* prior—are integrated as described in Sec. III. The implementation is in Python 3; simulations run in PyBullet [21] on a laptop with an Intel Core i7–1280P CPU. Videos and logs are provided in the supplementary material.

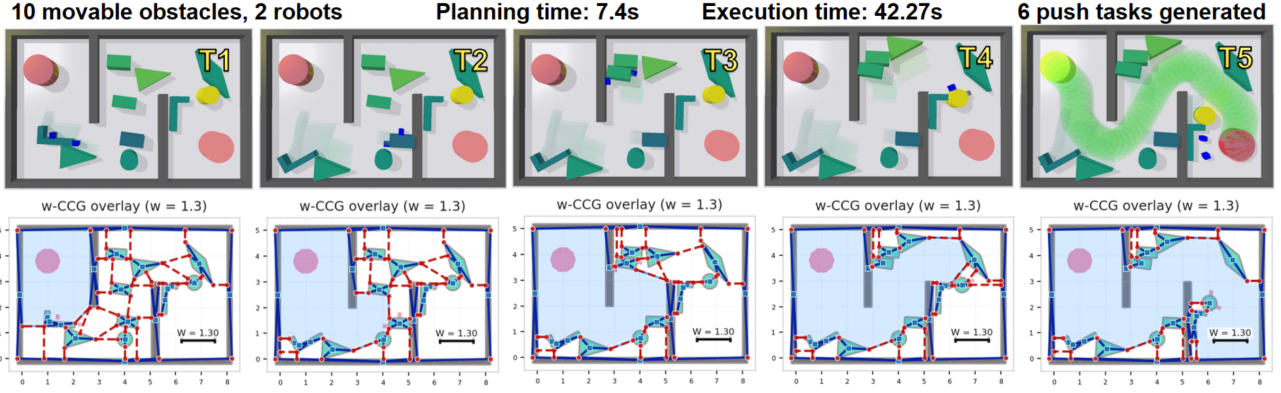


Fig. 6. Execution–planning alignment in the main scenario. **Top:** five PyBullet snapshots of the scene. **Bottom:** corresponding WCCG with the start face highlighted as a translucent blue polygon. The task moves a cylindrical object from the start $S = (1, 4)$ to the goal $G = (7, 2)$. In the final snapshot, the start face contains G , consistent with the green execution trajectory in the top row, confirming successful completion from S to G .

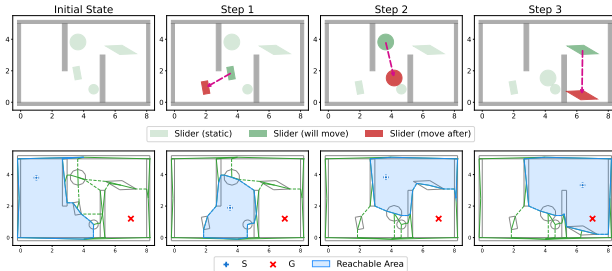


Fig. 7. Rec-NAMO. Sequentially builds path segments but often fails to form a complete W -clear path from start to goal. **Top:** pushing steps. **Bottom:** reachable region evolution.

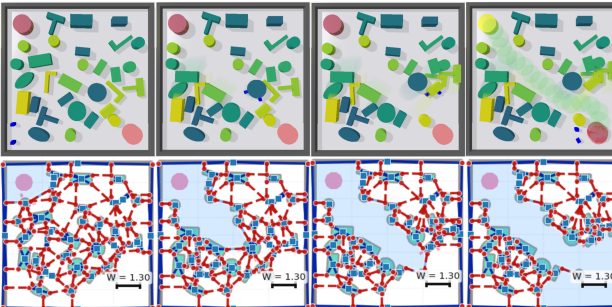


Fig. 8. Scalability in dense clutter (30 movables). **Top:** four execution snapshots as the robots clear bottlenecks and advance toward the goals. **Bottom:** corresponding WCCG overlays with the active face (translucent blue) and ranked gaps.

A. Numerical Simulations

1) Setup: The physics step is $\Delta t = 1/240$ s and the control period is $1/40$ s. Robots are modeled as disk/box pushers with risk radii consistent with the W -clearance definition. Movable obstacles have masses uniformly sampled from [5, 15] kg; immovables are modeled with mass 0. A trial succeeds when a W -clear path exists from start to goal and the target reaches its goal disc.

We use a *nominal scenario* with an 8×5 m bounded workspace, two internal bar obstacles (forming bottlenecks), and a mixed pool of curved and polygonal shapes (rings, ellipses, X/T/L/diamond, arrow-like, rectangles, cylinders). Two robots start in the lower-left; the goal lies on the right. Movables are randomly placed with a minimum separation. We test 10–15 objects across multiple random seeds.

2) Algorithm Configuration: Unless stated otherwise: the per-task simulation horizon is 80 steps; up to 64 candidate push tasks are generated per expansion; and the node priority is $f = g + \text{Cost}_{\text{to-go}}$ with heuristic factor 10. Gap sampling uses a softmax with temperature 0.05. *ModeTable* is enabled (auto-baked when missing). A *quick-pass* geometric screen may skip physics if a reference rollout already clears a gap; otherwise a short-horizon simulation with early stop is used. To avoid premature termination, a *deferred-reinsertion* rule retains high-value yet temporarily unexpanded nodes and revisits them later.

3) Baselines and Comparison: We compare against three representative families, all using the same W -clearance criterion and contact models:

(I) DFS-WCCG: a simulation-in-the-loop depth-first search sharing our physics predictor and W-CG for goal checking. Each node is a snapshot; actions are four fixed axis-aligned pushes $\leftarrow, \rightarrow, \uparrow, \downarrow$ applied to any movable (branching $\leq 4n$ for n objects).

(II) SL-Push: a straight-line (or waypointed) route where blockers are cleared by (i) offline minimal normal displacements or (ii) sim-in-the-loop normal pushes from near to far.

(III) Rec-NAMO: recursive routing/pushing on a cost-weighted visibility graph: Dijkstra for routing; local push decomposition for clearing; failures prune edges and trigger replanning.

Table I summarizes performance on the nominal scenario. DFS-WCCG suffers exponential growth of the search space as the number of movables increases, leading to long planning times and frequent timeouts (lowest success rate). SL-Push (offline) plans very quickly (< 0.1 s), but the lack of physics leads to physically unrealizable plans. Its sim-in-the-loop variant improves feasibility, but still requires many simulations and can produce unnecessarily long action sequences when the straight-line route is not the minimal pushing route; Fig. 7 illustrates a two-subgoal case. Rec-NAMO is faster than sim-in-the-loop approaches and effective for classical NAMO, yet it often fails to produce a fully connected W -clear route (Fig. 7), resulting in lower success.

By contrast, PIHS attains higher success with fewer simulations and lower planning/execution time due to (i) frontier-

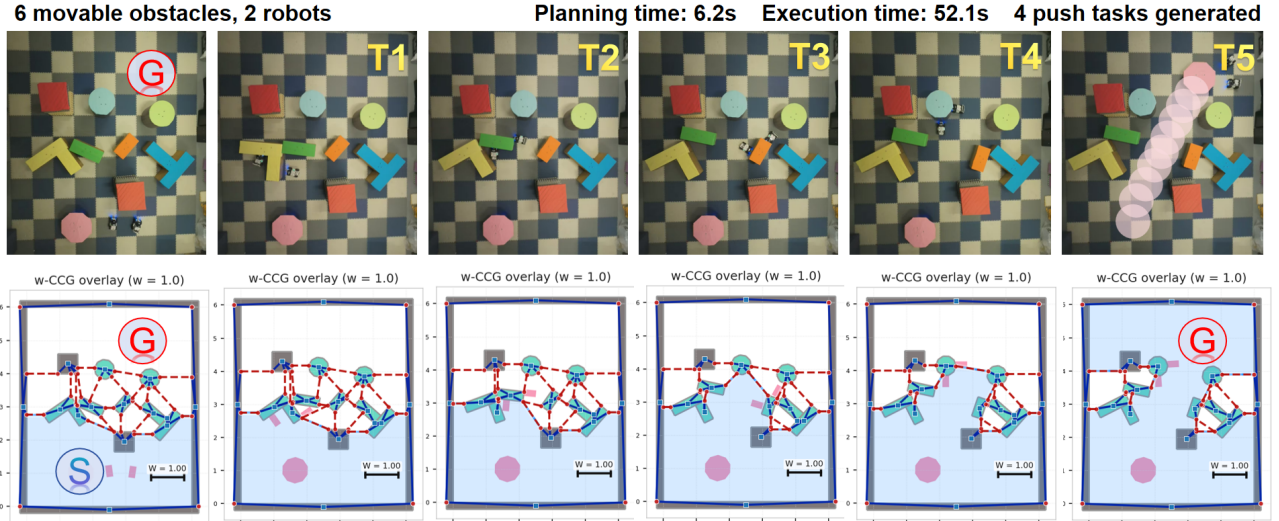


Fig. 9. Real-world pushing experiment with execution–planning alignment. **Top:** six snapshots as two robots push a target object in a 5×6 m workspace with both movable pieces and fixed boundaries. **Bottom:** corresponding WCCG overlays; the start face is highlighted in translucent blue. Planning uses clearance $W=1.0$, start $S=(1.65, 1.01)$, goal $G=(3.4, 4.8)$. The evolving graph and candidate gaps stay consistent with observed motions, indicating that planned corridors are compatible with execution.

based gap ranking, (ii) ModeTable-guided push directions, and (iii) quick-pass/early-stop. Deferred reinsertion further prevents priority-queue starvation by revisiting previously generated high-value nodes when a batch of actions fails.

4) Ablation Studies: Table II quantifies the contribution of each component by removing one factor at a time from SiLS. **Presearch** (frontier extraction + ranked gaps) is the largest time saver: without it, the planner invokes #Sims +56 and planning time increases by +6.6 s, while success drops by -7.5%. This confirms that presearch focuses expansions on high-yield gaps and avoids unproductive physics rollouts. **ModeTable** also provides a strong prior: removing it yields #Sims +42, #PT +4.8 s, and a -12.5% success drop, indicating the importance of structured contact-mode guidance beyond naive pushing heuristics. Disabling **quick-pass/early-stop** forces full-horizon simulation, increasing #Sims by +86 and #PT by +13.3 s, with only a minor success change (-2.5%); this shows that most expansions can be decided early without sacrificing feasibility. Finally, removing **deferred reinsertion** causes mild queue starvation (#Sims +29) and reduces success by -10.0%, highlighting the benefit of revisiting previously high-value nodes after local failures. Overall, each component contributes to either *efficiency* (fewer simulations, shorter planning time) or *robustness* (higher success), and the full SiLS configuration achieves the best trade-off across all metrics.

5) Dense-clutter scalability.: We further evaluate SiLS in a larger 8×5 m workspace populated with 30 movable objects. Despite the increased combinatorics, WCCG presearch and ModeTable guidance keep the branching small: the run in Fig. 8 completes with 10 node expansions (visited 115), 312 short simulation calls, and only 7 executed push tasks, yielding a connected W -clear corridor. Wall-clock planning takes 21.2 s and execution 24.5 s, after which all robots arrive at their goals. This illustrates that SiLS maintains efficiency and solution quality as scene density grows.

B. Hardware Experiments

1) System Description: As shown in Fig. 9, experiments are conducted in a $5 \text{ m} \times 6 \text{ m}$ workspace assembled from interlocking $0.6 \text{ m} \times 0.6 \text{ m}$ foam mats. Each trial uses two AgileX LIMO mobile robots and six movable obstacles (cardboard boxes covered with colored paper for visual distinction). Both robots and movables carry 3–4 motion-capture markers. A motion-capture system streams global poses to PyBullet in real time, enabling policy execution and visualization. Movables are randomly placed at the start of each trial to create diverse clutter.

2) Results: Figure 9 presents a representative real-world run. WCCG presearch finishes within 10 s, during which five gaps are sequentially cleared via 64 node expansions (maximum search depth = 3). In Task T1 (at $t=20$ s), a yellow T-shaped object is rotated counter-clockwise to expose a reachable contact on a neighboring green rectangle. In Task T2 (at $t=55$ s), the green rectangle is pushed to its target. Tasks T3 and T4 manipulate the orange rectangle and the blue cylinder, respectively, positioning them to open flanking gaps (at $t=71$ s and $t=77$ s). By Task T5, all gaps in the WCCG have been cleared, allowing a collision-free traverse from start to goal.

Execution time fluctuates due to occasional drifting/slippage of the Mecanum wheels at certain directions (near 45°), which lengthens some transitions and yields small discrepancies from simulation. To compensate, the system performs online replanning when needed. The temporal evolution of pushing actions and contact modes confirms that the planned interactions are physically realizable on hardware. Figure 9 and the supplementary videos provide additional qualitative evidence and the corresponding control traces.

V. CONCLUSION

This work introduces a multi-robot approach for path clearing in unstructured environments, utilizing a hybrid

search algorithm to plan and execute the sequence of obstacles, contact points, and forces efficiently. The framework demonstrates real-time adaptability to dynamic scenarios. Future work will address uncertainties such as estimating obstacle positions without external monitoring, handling uncertain obstacle masses, and managing partial robot visibility to improve robustness and performance in real-world, dynamic environments.

REFERENCES

- [1] L. Liu, X. Wang, X. Yang, H. Liu, J. Li, and P. Wang, “Path planning techniques for mobile robots: Review and prospect,” *Expert Systems with Applications*, vol. 227, p. 120254, 2023.
- [2] M. Stilman and J. J. Kuffner, “Navigation among movable obstacles: Real-time reasoning in complex environments,” *International Journal of Humanoid Robotics*, vol. 2, no. 04, pp. 479–503, 2005.
- [3] M. Stilman, J.-U. Schamburek, J. Kuffner, and T. Asfour, “Manipulation planning among movable obstacles,” in *Proceedings 2007 IEEE international conference on robotics and automation*. IEEE, 2007, pp. 3327–3332.
- [4] L. Yao, V. Modugno, A. M. Delfaki, Y. Liu, D. Stoyanov, and D. Kanoulas, “Local path planning among pushable objects based on reinforcement learning,” in *2024 IEEE/RSJ International Conference on Intelligent Robots and Systems (IROS)*. IEEE, 2024, pp. 3062–3068.
- [5] Z. Tang, Y. Feng, and M. Guo, “Collaborative planar pushing of polytopic objects with multiple robots in complex scenes,” *arXiv preprint arXiv:2405.07908*, 2024.
- [6] Z. Ren, B. Suvonov, G. Chen, B. He, Y. Liao, C. Fermuller, and J. Zhang, “Search-based path planning in interactive environments among movable obstacles,” in *2025 IEEE International Conference on Robotics and Automation (ICRA)*. IEEE, 2025, pp. 533–539.
- [7] S. Goyal, A. Ruina, and J. Papadopoulos, “Limit surface and moment function descriptions of planar sliding,” in *IEEE International Conference on Robotics and Automation (ICRA)*, 1989, pp. 794–795.
- [8] K. M. Lynch, H. Maekawa, and K. Tanie, “Manipulation and active sensing by pushing using tactile feedback.” in *IROS*, vol. 1, 1992, pp. 416–421.
- [9] R. Ni and A. H. Qureshi, “Progressive learning for physics-informed neural motion planning,” *arXiv preprint arXiv:2306.00616*, 2023.
- [10] Y. Liu, R. Ni, and A. H. Qureshi, “Physics-informed neural mapping and motion planning in unknown environments,” *IEEE Transactions on Robotics*, 2025.
- [11] J. Chen, M. Gauci, W. Li, A. Kolling, and R. Groß, “Occlusion-based cooperative transport with a swarm of miniature mobile robots,” *IEEE Transactions on Robotics*, vol. 31, no. 2, pp. 307–321, 2015.
- [12] R. Ni and A. H. Qureshi, “Physics-informed neural motion planning on constraint manifolds,” in *2024 IEEE International Conference on Robotics and Automation (ICRA)*. IEEE, 2024, pp. 12 179–12 185.
- [13] Y. Wang and C. W. De Silva, “Multi-robot box-pushing: Single-agent q-learning vs. team q-learning,” in *2006 IEEE/RSJ international conference on intelligent robots and systems*, 2006, pp. 3694–3699.
- [14] Y. Feng, C. Hong, Y. Niu, S. Liu, Y. Yang, and D. Zhao, “Learning multi-agent loco-manipulation for long-horizon quadrupedal pushing,” in *2025 IEEE International Conference on Robotics and Automation (ICRA)*. IEEE, 2025, pp. 14 441–14 448.
- [15] Y.-C. Lin, B. Ponton, L. Righetti, and D. Berenson, “Efficient humanoid contact planning using learned centroidal dynamics prediction,” in *2019 International Conference on Robotics and Automation (ICRA)*. IEEE, 2019, pp. 5280–5286.
- [16] Q. Rouxel, S. Ivaldi, and J.-B. Mouret, “Multi-contact whole-body force control for position-controlled robots,” *IEEE Robotics and Automation Letters*, vol. 9, no. 6, pp. 5639–5646, 2024.
- [17] F. Hou and *[Coauthors]*, “physics-based planning for non-prehensile manipulation / exact title,” in *Conference (e.g., ICRA/ICRA Workshop/IROS)*, 2020, pp. [pp–pp]. [Online]. Available: ⟨pdf-or-arXiv-link⟩
- [18] P. Agrawal, A. Nair, and P. Abbeel, “Learning to poke by poking: Experiential learning of intuitive physics,” *arXiv preprint arXiv:1606.07419*, 2016. [Online]. Available: <https://arxiv.org/abs/1606.07419>
- [19] Z. Tang, J. Chen, and M. Guo, “Combinatorial-hybrid optimization for multi-agent systems under collaborative tasks,” in *IEEE Conference on Decision and Control (CDC)*, 2023.
- [20] K. N. McGuire, G. C. H. E. de Croon, and K. Tuyls, “A comparative study of bug algorithms for robot navigation,” *Robotics and Autonomous Systems*, vol. 121, p. 103261, 2019.
- [21] E. Coumans and Y. Bai, “Pybullet, a python module for physics simulation for games, robotics and machine learning,” <http://pybullet.org>, 2016–2019.